Send Orders for Reprints to reprints@benthamscience.net

Protein & Peptide Letters, **2026,** ***33*****, 379-393**

RESEARCH ARTICLE

Dimerization of SARS-CoV-2 3CLpro and the Role of the A7G/V125G Zipper Interface

Rafida Razali[1], Cahyo Budiman[2,*] and Vijay Kumar[2]

[1]*Faculty of Resource Science and Technology, Universiti Malaysia Sarawak, Jalan Datuk Mohammad Musa, 94300 Kota Samarahan, Sarawak, Malaysia;* [2]*Biotechnology Research Institute, Universiti Malaysia Sabah, 88400, Kota Kinabalu, Sabah, Malaysia*

ARTICLE HISTORY

Received: August 28, 2025
Revised: January 15, 2026
Accepted: January 20, 2026

DOI:
10.2174/0109298665442327260216063524

Abstract: ***Introduction/Objectives*****:** The 3-chymotrypsin-like protease (3CLpro) of severe acute respiratory syndrome coronavirus 2 (SARS-CoV-2) is essential for viral replication and is catalytically active only in its dimeric form. Elucidating the molecular determinants that stabilize this dimer may uncover novel antiviral drug targets. This study aimed to characterize the oligomerization behavior of wild-type 3CLpro and to elucidate the functional role of an alanine–valine zipper motif in dimer stability and enzymatic activity.

Methods**:** Wild-type 3CLpro (3CLpro-WT) was heterologously expressed in *Escherichia coli* BL21(DE3) and purified by nickel-affinity chromatography. Oligomerization behavior was examined using Size-Exclusion Chromatography (SEC) under varying protein concentrations, pH conditions, and ionic strengths. An alanine–valine zipper mutant (A7G/V125G; 3CLpro-ZM) was generated by site-directed mutagenesis, overexpressed, purified using the same protocol, and analyzed for changes in folding, oligomerization, and enzymatic activity.

Results**:** 3CLpro-WT predominantly existed as a stable dimer, independent of protein concentration and ionic strength, but was destabilized under extreme pH conditions. In contrast, 3CLpro-ZM exhibited a perturbed dimerization equilibrium, altered secondary structure, and a pronounced reduction in both protease and esterase activities compared with the wild-type enzyme.

Discussion**:** These findings demonstrate that hydrophobic interactions are the primary force stabilizing the 3CLpro dimer, while ionic interactions provide pH-sensitive modulation. Disruption of the alanine–valine zipper compromises dimer integrity and allosterically impairs catalytic activity, despite the mutation being distant from the active site.

Conclusion**:** The Ala7–Val125 interface contributes to 3CLpro stability and activity and may be a promising site for future allosteric inhibitor design.

Keywords: SARS-CoV-2, 3CLpro, dimerization, alanine-valine zipper, site-directed mutagenesis, oligomerization.

1. INTRODUCTION

In late December 2019, the emergence of a pneumonia-like disease was reported in Wuhan, China, marking the beginning of a global health crisis [1, 2]. Since then, this infectious disease, caused by Severe Acute Respiratory Syndrome Coronavirus 2 (SARS-CoV-2), has rapidly escalated into a pandemic, prompting the World Health Organization (WHO) to declare a Public Health Emergency of International Concern (PHEIC) on January 30, 2020, followed by a pandemic declaration on March 11, 2020 [3]. Although the WHO officially declared an end to the COVID-19 PHEIC on May 5, 2023, it is imperative that global awareness continues to recognize COVID-19 as an ongoing global health threat, with numerous severe cases and fatalities still occurring around the world [4]. Therefore**,** the development of effective antiviral drugs remains crucial to address this ongoing need.

The SARS-CoV-2 genome encodes two large polyproteins, pp1a and pp1ab, which are cleaved by viral proteases into functional non-structural proteins essential for viral replication and assembly [5]. Among these proteases, the 3-chymotrypsin-like protease (3CLpro), also known as the Main protease (Mpro), plays an important role in cleaving these polyproteins at multiple sites [5]. The functional significance of 3CLpro in the viral life cycle, coupled with the absence of closely related homologs in humans, identifies 3CLpro as an attractive target for the design of antiviral drugs [1, 6, 7]. Furthermore, the highly conserved three-dimensional structure across various Coronavirus (CoV) strains, including SARS-CoV-1 and

*Address correspondence to this author at the Biotechnology Research Institute, Universiti Malaysia Sabah, 88400 Kota Kinabalu, Sabah, Malaysia; E-mail: cahyo@ums.edu.my

0929-8665/26 $65.00+.00

MERS-CoV, makes it an appealing target for the development of broad-spectrum therapeutic agents [8]. This high level of conservation is particularly advantageous as mutations in such critical viral proteins are often lethal to the virus, suggesting that drugs specifically targeting conserved 3CLpro regions have the potential to inhibit viral replication and proliferation effectively, thereby helping to mitigate the risk of drug resistance [9].

A fundamental aspect of SARS-CoV-2 3CLpro's function is its enzymatic activity, which is observed in its dimeric form. The catalytic dyad, comprising His41 and Cys145, becomes fully functional only upon dimerization [10, 11]. This dimerization is structurally critical, as the N-finger of each monomer interacts with Glu166 of the opposing monomer, facilitating the correct orientation of the S1 pocket within the substrate-binding site [10]. Previous structural analyses, particularly X-ray crystallography studies, have indicated that the dimerization of 3CLpro is primarily mediated by a combination of hydrogen bonding and hydrophobic interactions at the dimer interface [12].

For the development of antiviral drugs, researchers have employed two primary strategies for inhibiting 3CLpro: (i) the design of molecules that directly target the substrate-binding pocket to block catalytic activity, and (ii) the development of inhibitors that specifically disrupt the enzyme's dimerization. While numerous studies have focused on inhibitors that can block the active site, with several compounds showing promise and advancing to clinical trials, studies exploring inhibitors that target 3CLpro's dimerization remain comparatively limited. This disparity highlights a significant knowledge gap, as a deeper understanding of 3CLpro dimerization is crucial for the development of therapeutic approaches. Targeting the dimerization interface offers distinct advantages over active-site inhibition. Active-site inhibitors, despite targeting conserved regions, can still face challenges with viral evolution, leading to resistance mutations or off-target effects. In contrast, dimerization inhibitors often function through an allosteric mechanism, which can provide a broader spectrum of activity and potentially reduce the likelihood of resistance development, as the binding site is not directly involved in catalysis. Research on the successful development of specific compounds that disrupt 3CLpro dimerization is currently ongoing; however, the dimerization inhibitors are effective in preventing the disease progression in pathological contexts [13].

The 3CLpro dimer interface contains an intriguing structural feature known as an Alanine-Valine knot, in which Ala7 and Val125 from one monomer interact reciprocally with Val125 and Ala7 from the opposing monomer, forming a zipper-like arrangement that contributes to stabilization of the dimer interface [10]. This motif is particularly noteworthy given that hydrophobic zippers are well-documented in protein dimerization, typically involving residues like Leucine or Valine, with aliphatic hydrophobic residues such as Alanine and Valine playing an important role in promoting protein association [14, 15]. However, despite its structural prominence, the precise functional role of this Ala7-Val125 zipper in the 3CLpro dimerization process has remained underexplored. Addressing this underexplored aspect is essential for understanding the complexities of the function of 3CLpro and identifying new therapeutic pathways. Notably, previous studies on 3CLpro of SARS-CoV and SARS-CoV-2 have primarily focused on mutagenesis of residues surrounding the catalytic site or key interfacial residues involved in substrate binding and N-finger stabilization, such as Glu166 and residues shaping the S1 pocket. Although these studies demonstrated the significance of dimerization for enzymatic activity, they did not specifically investigate the functional role of small aliphatic residues that create hydrophobic zipper-like motifs at the dimer interface. However, to evaluate its role in dimer stability and allosteric regulation of catalytic activity, the present study particularly focuses on the Ala7/Val125 interface, a structurally conserved yet underexplored alanine–valine zipper.

Therefore, this study aims to comprehensively explore the oligomerization behavior of recombinant SARS-CoV-2 3CLpro. Utilizing size-exclusion chromatography, the research investigates the effects of critical environmental variables, including ionic strength, pH, and protein concentration, on the oligomeric state of the wild-type enzyme. Furthermore, the study analyses the impact of specific mutations within the dimeric interface, focusing on the Ala7-Val125 zipper residues. The main objective is to obtain valuable insight into the dimerization mechanism of SARS-CoV-2 3CLpro, which can directly contribute to the rational design and development of novel antiviral drugs specifically targeting its dimeric interface.

2. MATERIALS AND METHODS

2.1. Expression of 3CLpro Wild Type

The expression system for 3CLpro wild type (3CLpro-WT) was generously provided by Dr. Andrey Kovalevsky (Oak Ridge National Laboratory, Tennessee, U.S.A.), with the protocol for its use detailed by Kneller *et al.* (2020) [16]. In this system, the gene encoding 3CLpro-WT was integrated into the pD451-SR plasmid, resulting in the pD451-3CLpro expression system. Under this system, the target protein (3CLpro-WT) is intended to be expressed as an N-terminal Maltose-Binding Protein (MBP) fusion with a C-terminal 6×His tag, resulting in a theoretical molecular mass of approximately 79 kDa before processing. A linker sequence (LINGDGAGLEVLSAVLQ), positioned between MBP and 3CLpro-WT, functions as an autocleavage site recognized by 3CLpro itself. This expression system plasmid was subsequently transformed into *Escherichia coli* strain BL21(DE3) (Sigma-Aldrich, MA, USA) using the heat-shock method [17]. Positive transformants were selected and cultured in Luria Bertani (LB) (BD Difco, Sparks, MD, USA) medium supplemented with 35 μg/mL kanamycin (Merck KGaA, Darmstadt, Germany) at 37^{o}C, with agitation at 180 rpm, overnight [18]. A 2% inoculum from these bacterial suspensions was then transferred to a larger culture volume of LB medium containing the antibiotic and incubated at 37^{o}C with agitation at 180 rpm. Protein expression was induced by the addition of 1 mM isopropyl-D-1-thiogalactosidase (IPTG) (Merck KGaA, Darmstadt, Germany) once the optical density at 600nm (OD600nm) reached 0.8, followed by overnight incubation at 18^{o}C with

agitation at 180 rpm. The OD600nm was measured using a PerkinElmer Lambda 25 UV/Vis Spectrometer (Waltham, MA, USA). All incubations were conducted using a floor-model refrigerated incubated shaker (IS-971R; JeioTech Co., Ltd., Daejeon, South Korea).

2.2. Cell Harvesting

Cells were harvested by centrifugation at 8,000 x g at 4°C for 10 minutes, followed by thorough washing to remove residual medium [19]. The washed cell pellet was then resuspended in a lysis buffer and subjected to sonication on ice to disrupt the cells. Cell debris was subsequently removed by ultracentrifugation at 35,000 × g (Beckman Optima L-100K, Brea, CA, USA) for 30 minutes at 4°C. The resulting supernatant, containing the soluble protein fraction, was collected and used for subsequent purification steps.

2.3. Protein Purification

The expressed soluble 3CLpro-WT was purified using nickel-affinity chromatography performed on an ÄKTA™ Pure liquid chromatography system (GE Healthcare, Chicago, IL, USA). Purification was carried out under identical flow-rate conditions for all protein samples. A 5 mL HisTrap™ HP column prepacked with Ni^{2+}-charged resin (GE Healthcare, Chicago, IL, USA) was equilibrated with lysis buffer consisting of 20 mM Tris-HCl (Sigma-Aldrich, St. Louis, MO, USA) adjusted to pH 8.0, 40 mM imidazole (Sigma-Aldrich, St. Louis, MO, USA), 150 mM sodium chloride (Merck, Darmstadt, Germany), and 1 mM dithiothreitol (DTT; Thermo Fisher Scientific, Waltham, MA, USA). Prior to column loading, the clarified soluble protein fractions were passed through a 0.22 µm syringe filter (Millipore, Burlington, MA, USA) to remove particulate contaminants. Filtered samples were then applied to the column at a flow rate of 1.0 mL/min. Bound proteins were eluted using a linear imidazole gradient ranging from 0 to 500 mM in elution buffer containing 20 mM Tris-HCl (pH 8.0), 150 mM NaCl, and 1 mM DTT, prepared using the same reagent sources as described above.

2.4. SDS-PAGE Analysis

The expression, solubility, and purity of the target proteins were confirmed using 15% Sodium Dodecyl Sulfate-Polyacrylamide Gel Electrophoresis (SDS-PAGE). The method followed that described by Laemmli (1970), with minor modifications [20]. The gels consisted of a 6% (v/v) stacking gel and a 15% (*v/v*) resolving gel prepared using acrylamide/bis-acrylamide solution (30%, Bio-Rad Laboratories Inc., Hercules, CA, USA). Gel polymerization was initiated by the addition of ammonium persulfate (APS) and *N,N,N′,N′*-tetramethylethylenediamine (TEMED) (Sigma-Aldrich, St. Louis, MO, USA). Electrophoresis was performed using a Mini-PROTEAN® Tetra Cell system connected to a PowerPac™ Basic power supply (Bio-Rad Laboratories Inc., Hercules, CA, USA). Prior to electrophoresis, protein samples were mixed with Laemmli sample buffer (Bio-Rad Laboratories Inc., Hercules, CA, USA) containing SDS and reducing agent, followed by heat denaturation at 95°C for 5 min. Equal volumes of denatured samples were loaded into each well together with a low molecular weight protein marker (Calibration Kit Low Molecular Weight, Cytiva, Marlborough, MA, USA), covering a molecular mass range of 14.4–97.0 kDa.

Electrophoretic separation was carried out at a constant voltage of 150 V using 1× SDS running buffer (25 mM Tris, 192 mM glycine, and 0.1% SDS) until the dye front reached the bottom of the gel. Following separation, the gels were stained with Coomassie Brilliant Blue R-250 staining solution (Bio-Rad Laboratories Inc., Hercules, CA, USA) and subsequently destained using a methanol–acetic acid-based destaining solution until clear protein bands were observed. The stained gels were finally visualized and documented using a Gel Doc™ XR+ imaging system (Bio-Rad Laboratories Inc., Hercules, CA, USA).

2.5. Oligomeric States of 3CLpro-WT (Effect of Ionic Strength, pH, and Protein Concentration)

The oligomerization profile of 3CLpro-WT was analyzed by Size-Exclusion Chromatography (SEC) using an ÄKTA FPLC purification system (GE Healthcare, Illinois, USA) equipped with a HiLoad™ 16/600 Superdex™ 200 pg column (Cytiva, Marlborough, USA). Prior to SEC analysis, the purified 3CLpro-WT fraction was collected and concentrated to 2 mg/mL. To evaluate the effect of ionic strength on oligomerization, the concentrated protein was dialyzed overnight at 4°C against buffers containing different NaCl concentrations (20 mM Tris-HCl, pH 8.0, supplemented with 150, 300, or 500 mM NaCl). To assess the effect of pH, the protein was dialyzed overnight at 4°C against buffers of varying pH (20 mM Tris-HCl, pH 5.0, 8.0, or 10.0, each containing 150 mM NaCl). Following dialysis, samples were subjected to SEC using the corresponding dialysis buffer.

To investigate the influence of protein concentration on the oligomeric state of 3CLpro-WT, the purified protein was concentrated to final concentrations of 4, 2, 1, and 0.2 mg/mL. Aliquots of 100 µL were injected into the column and eluted with 20 mM Tris-HCl (pH 8.0) containing 150 mM NaCl [21]. All samples were eluted at a constant flow rate of 1.0 mL/min, and elution profiles were monitored at 280 nm. The column was calibrated using a Gel Filtration Markers Kit for Protein Molecular Weights (12–200 kDa; Sigma-Aldrich, St. Louis, USA). Calibration curves were generated by plotting the logarithm of molecular mass against the partition coefficient, calculated as $(Ve - V0)/(Vt - V0)$, where Ve is the elution volume, V0 is the void volume, and Vt is the total bed volume. Proteins of known molecular mass were analyzed under identical conditions to estimate the apparent molecular mass of 3CLpro-WT at different salt concentrations, pH values, and protein concentrations.

2.6. Construction of 3CLpro Zipper Mutant

The 3CL protease zipper mutant (3CLpro-ZM) was generated by simultaneous substitution of alanine at position 7 and valine at position 125 with glycine, yielding the A7G and V125G double mutant (Figure **1**). Site-directed mutagenesis was carried out using the KOD-Plus-Mutagenesis Kit (Toyobo Co., Ltd., Osaka, Japan), which employs a high-fidelity KOD DNA polymerase–based

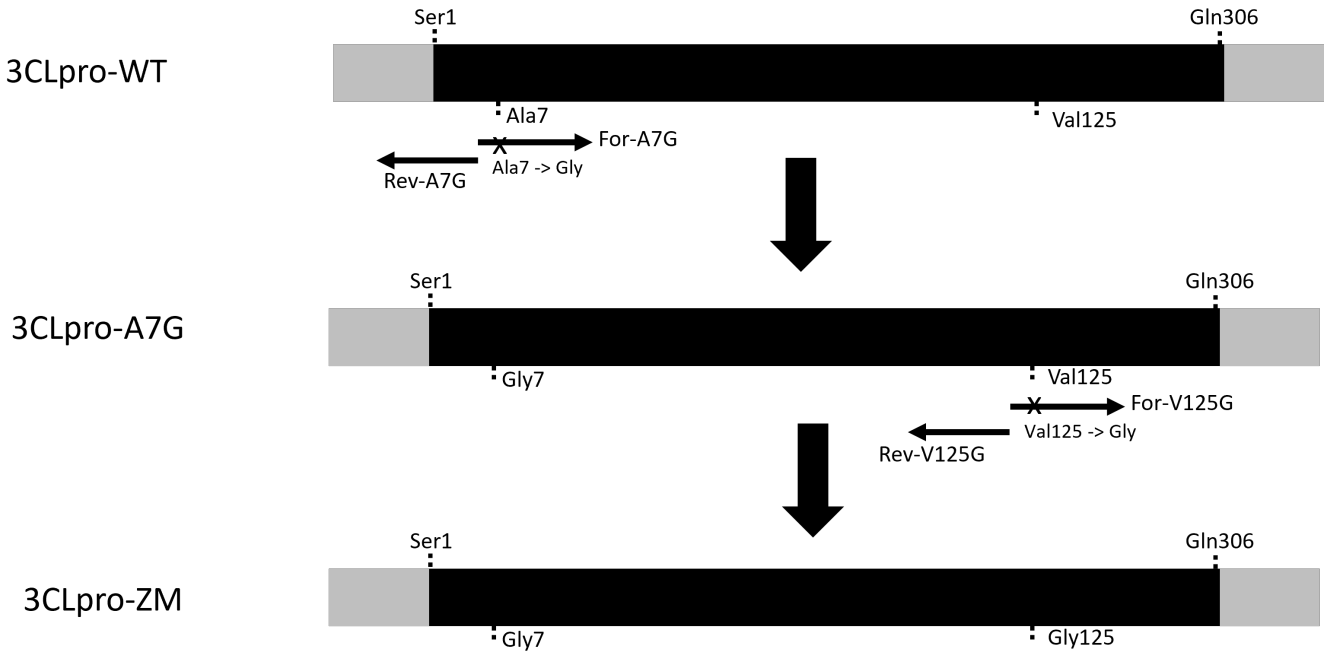

Figure 1. Construction of 3CLpro-ZM. *(A higher resolution / colour version of this figure is available in the electronic copy of the article).*

inverse PCR strategy, according to the manufacturer's protocol with minor modifications. Inverse PCR was performed using mutagenic primers (10 pmol each) designed to introduce the desired nucleotide substitutions, with approximately 50 ng of methylated parental plasmid as template. Amplification was conducted using KOD-Plus DNA polymerase (1 U per reaction; Toyobo Co., Ltd., Osaka, Japan) supplied in the kit. Following PCR, the parental plasmid DNA was selectively removed by digestion with DpnI restriction enzyme (20 U per reaction; Toyobo Co., Ltd., Osaka, Japan) at 37°C for 1 h. The resulting PCR products were subsequently phosphorylated and self-ligated using T4 polynucleotide kinase (5 U per reaction; Toyobo Co., Ltd., Osaka, Japan) and T4 DNA ligase (provided as ligation high mixture; Toyobo Co., Ltd., Osaka, Japan), according to the kit instructions. The ligation products were transformed into *Escherichia coli* competent cells, and positive clones were selected and verified by DNA sequencing to confirm the presence of the intended mutations and the absence of secondary mutations. The nucleotide sequences of the primers used are listed in Table **1**.

The confirmed 3CLpro-ZM gene was subsequently subcloned into the pMAL-p5X expression vector (New England Biolabs, Ipswich, MA, USA) using the restriction enzymes BamHI and HindIII (10 U each per digestion; Toyobo Co., Ltd., Osaka, Japan). The construct was designed to encode an N-terminal Maltose-Binding Protein (MBP) fusion to enhance protein expression and solubility, followed by an engineered autocleavage sequence (LINGDGAGLEVLSAVLQ) as in its wild type. This configuration enabled removal of the MBP tag during protein processing, yielding the untagged 3CLpro-ZM. A C-terminal hexahistidine (6×His) tag was retained to facilitate affinity purification and downstream biochemical characterization.

Table 1. Primers for site-directed mutagenesis.

Primer	Sequence
Forward A7G	5'-GAA GGT TGT ATG GTT CAG GTA ACC TGC GGC ACT-'3
Reverse A7G	5'-AGA ACC GTT ATA GCA AGC CAG AAC GCT GAA GGT CTG AC–'3
Forward V125G	5'-CCG TCT GGT GGT TAC CAG TGC GCT ATG CGT–'3
Reverse V125G	5'-AGA ACC GTT ATA GCA AGC CAG AAC GCT GAA GGT CTG AC–'3

2.7. Overexpression and Purification of 3CLpro-ZM

The expression vector encoding 3CLpro-ZM was transformed into *Escherichia coli* BL21(DE3) cells (Sigma-Aldrich, St. Louis, MO, USA) using a protocol analogous to that employed for the wild-type protein. A 10 mL starter culture of *E. coli* BL21(DE3) harboring the 3CLpro-ZM plasmid was inoculated from a single colony on a freshly streaked LB agar plate supplemented with 100 µg/mL ampicillin (Sigma-Aldrich, St. Louis, MO, USA). Following overnight incubation at 37°C with orbital shaking at 180 rpm, 2% (*v/v*) of the starter culture was transferred into a larger volume of LB medium (BD Difco, Sparks, MD, USA) containing the same antibiotic and incubated under identical conditions.

Protein expression was induced by the addition of isopropyl β-D-1-thiogalactopyranoside (IPTG; Sigma-Aldrich, St. Louis, MO, USA) to a final concentration of 1 mM when the culture reached an OD_{600} of approximately 0.8, as measured using a UV–Vis spectrophotometer (BioSpectrometer®, Eppendorf, Hamburg, Germany). The

cultures were then incubated overnight at 18°C with shaking at 180 rpm. Cells were harvested by centrifugation using a refrigerated centrifuge (Avanti J-26 XP, Beckman Coulter, Brea, CA, USA), lysed by sonication on ice using a probe sonicator (Q125 Sonicator, Qsonica, Newtown, CT, USA), and the recombinant protein was purified by Ni^{2+}–NTA affinity chromatography according to the method for 3CLpro-WT.

2.8. Oligomeric States of 3CLpro-ZM

The oligomerization states of 3CLpro-ZM proteins were determined using a methodology analogous to that employed for 3CLpro-WT using protein samples at concentrations of 4 and 2 mg/ml. A volume of 100 µl of each sample was introduced into the chromatographic column, followed by elution using a buffer solution at a flow rate of 1.0 ml/min, and other technical parameters follow the wild type. The SEC buffer composition for 3CLpro-ZM oligomerization analysis consisted of 20 mM Tris-HCl and 150 mM NaCl, adjusted to a pH of 8.0.

2.9. Far UV Circular Dichroism (CD) Spectra of 3CLpro-WT and 3CLpro-ZM

Far UV CD spectra were measured using a J-725 automatic spectropolarimeter (JASCO, Tokyo, Japan) at 10°C. Purified proteins were dissolved in 20 mM sodium phosphate (pH 8.0) at a concentration of 0.2 mg/ml, utilizing a cell with an optical path length of 2 mm (Hellma Analytics, Müllheim, Baden-Württemberg, Germany). Prior to measurement, protein samples were incubated at 10°C for 30 minutes. The far UV CD spectra were recorded from 190 nm to 250 nm wavelengths. The mean residue ellipticity θ (deg cm^2/dmol) was calculated using an average amino acid molecular mass of 110 [14]. Secondary structure content was estimated following Yang's methodology [22, 23].

2.10. Protease activity of 3CLpro-WT and 3CLpro-ZM

The protease activity of the proteins was determined based on the method described by Cheng *et al.* (2010) [24]. Activity was measured using a calorimetry-based peptide cleavage assay with the 6-mer peptide substrate TSAVLQ-para-nitroanilide (TQ6-pNA; Bachem, Bubendorf, Basel-Landschaft, Switzerland), as previously prescribed [18]. TSAVLQ represents the nsp4↓nsp5 cleavage sequence for SARS and SARS-CoV-2 3CLpro [25]. The reaction mixture was 100 µL and contained 10 mM phosphate buffer (pH 7.6), 25 µM TQ6-pNA substrate, and 0.5 µM of enzyme. The enzyme was pre-incubated in the reaction buffer for 10 minutes at 30°C before substrate addition. The reaction was initiated by the addition of substrate and allowed to proceed for an additional 10 minutes. The release of p-nitroanilide was quantified by measuring absorbance at 405 nm using a Tecan Sunrise absorbance microplate reader (Tecan, Morrisville, NC, USA). Product concentration was calculated using a molar extinction coefficient of 9,800 $M^{-1} \cdot cm^{-1}$. One unit of protease activity was defined as the amount of enzyme required to produce 1 µmol of product per minute under the assay conditions.

2.11. Esterase activity of 3CLpro-WT and 3CLpro-ZM

The esterase activity of the proteins was determined following the same general methodology as the protease activity assay [18]. *N*-carbobenzoxyglycine *p*-nitrophenyl ester (N-CBZ-Gly-pNP; Sigma-Aldrich, St. Louis, MO, USA) was used as the substrate, in which cleavage of the Gly-pNP bond releases free *p*-nitrophenol (pNP), resulting in an increase in absorbance at 340 nm. Absorbance was monitored using a Tecan Sunrise absorbance microplate reader (Tecan, Männedorf, Switzerland). The esterase assay was performed in a 100 µL reaction cocktail composed of 10 mM phosphate buffer, pH 7.6, containing 25 µM N-CBZ-Gly-pNP and 0.5 µM of enzyme, and the reaction was carried out at 30°C for 10 minutes. Prior to substrate addition, the enzyme was pre-incubated in buffer for 10 minutes at 30°C. Esterase activity was calculated using the Beer–Lambert law, with a molar absorption coefficient of 6,320 M^{-1} cm^{-1} at 340 nm. One unit of esterase activity was defined as the amount of enzyme required to produce 1 µmol of product per minute.

2.12. Data Analysis

Quantitative data are presented as the mean ± standard deviation of three independent biological replicates. Data analysis was performed descriptively by comparing trends, distributions, and relative differences among experimental conditions.

3. RESULTS AND DISCUSSIONS

3.1. Production of 3CLpro-WT

Figure **2** shows the expression of 3CLpro-WT analyzed by 15% SDS–PAGE using *E. coli* BL21(DE3) as the host cell. The results indicate that the protein was successfully expressed heterologously in this system. This is evidenced by the appearance of a distinct band at approximately 35 kDa, which corresponds well to the theoretical molecular mass of 3CLpro-WT with a C-terminal 6×His tag and without the MBP fusion tag, observed in the cell fraction after IPTG induction. No band of similar size was detected before IPTG induction, clearly confirming that this band represents the expressed target protein. The 3CLpro-WT band also showed much higher intensity compared to endogenous *E. coli* proteins, indicating strong overexpression and substantial accumulation of the recombinant protein. Notably, the observed molecular mass did not match the expected size of the full MBP–3CLpro-WT–6×His fusion protein, which is approximately 77 kDa. This difference suggests that the MBP tag was autocleaved during expression, producing a free MBP band at around 42 kDa and a separate 3CLpro-WT–6×His band at approximately 37 kDa. Consistent with this, Figure **2** shows a prominent band near 42 kDa, which likely corresponds to the cleaved MBP. As a result, the mature 3CLpro-WT was obtained with a free N-terminus and only a minimal C-terminal His tag. This expression strategy ensures that the biochemical properties and oligomerization behavior observed for 3CLpro-WT reflect the intrinsic characteristics of the mature protease, rather than effects caused by fusion partners. Furthermore, Figure **2** shows that the 3CLpro-WT

band was present only in the soluble fraction and not in the insoluble (pellet) fraction. This indicates that the expressed protein was fully soluble. These results are consistent with a previous report showing that the MBP fusion strategy is effective for producing soluble 3CLpro-WT in heterologous expression systems [18].

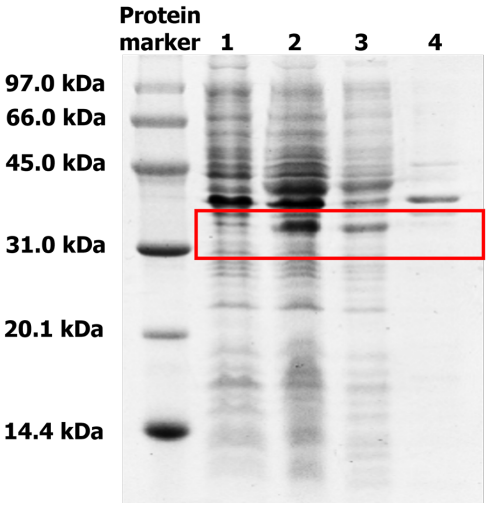

Figure 2 Expression check of 3CLpro-WT visualized under 15% SDS-PAGE. Lane 1: Before IPTG induction; Lane 2: After IPTG induction; Lane 3: Soluble fraction obtained after the sonication; Lane 4: Insoluble fraction obtained after the sonication. The red box highlights the location of the recombinant proteins. *(A higher resolution / colour version of this figure is available in the electronic copy of the article).*

The subsequent step of purification of this protein was implemented using Ni^{2+}-NTA affinity chromatography after the successful completion of fully soluble expression. The single bands were obtained following this chromatography stage, as illustrated in Figure (**3**), indicating that 3CLpro-WT was successfully purified under a single chromatography step. The SDS-PAGE did not reveal any visible contaminants, indicating that the protein was of high purity. This is advantageous for subsequent analysis. It is important to note that the chromatography technique chosen was based on the expression design of the protein, which includes a 6xHis-tag at the N-terminus.

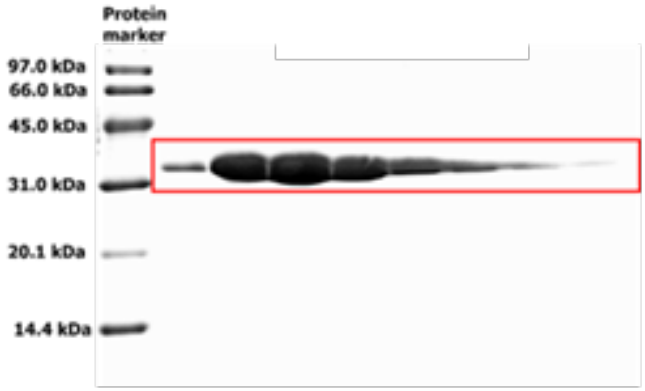

Figure 3. Purification checks of 3CLpro-WT visualized under 15% SDS-PAGE after Ni^{2+}-NTA chromatography. *(A higher resolution / colour version of this figure is available in the electronic copy of the article).*

3.2. Oligomeric state of 3CLpro WT: Effect of NaCl and pH

The dimeric structure of SARS-CoV-2 3CLpro is necessary for it to work as a catalyst. Consequently, a thorough comprehension of the factors that affect or destabilize this dimeric structure is essential, as these disruptions directly influence the enzyme's ability to process viral polyproteins and so serve as prospective targets for antiviral inhibitors. For this purpose, the effects of different ionic strengths, pH levels, and protein concentrations on the oligomeric state of 3CLpro-WT in solution were meticulously analyzed using Size-Exclusion Chromatography (SEC).

The oligomerization investigation of 3CLpro-WT, conducted at an initial protein concentration of 2 mg/ml, yielded essential insights into its behavior in solution. Figure **4** shows how the protein's oligomeric state changes with the amount of salt. Even though the NaCl concentrations increased from 150 mM to 500 mM, the dimeric structure of 3CLpro-WT stayed the same, with only small changes in the elution profiles. In these settings, 3CLpro-WT always eluted at an elution volume of about 79 mL, which is about 72 kDa in apparent molecular mass. This result is about twice the theoretical molecular mass of the monomer (35 kDa), which indicates that under these conditions, the protein mostly existed as a stable dimer. It is important to note that SEC analysis was conducted under lower ionic strength conditions (<150 mM) in this study. Therefore, while the data suggest that dimer stability is preserved at moderate to high salt concentrations, additional investigations at lower ionic strength would be beneficial to comprehensively elucidate the role of electrostatic interactions in 3CLpro dimerization. This data clearly indicates that ionic strength exerts an insignificant influence on the stability of the 3CLpro dimer. It is interesting to note that raising the ionic strength from 150 to 500 mM NaCl did not change the elution volume in a significant way. This shows that strong electrostatic interactions are not likely to be the main mechanism that keeps 3CLpro dimerization stable under these conditions. Nonetheless, this does not preclude the influence of electrostatic interactions entirely. Residual ionic interactions may still work locally at the dimer interface and be functionally important, especially when the ionic strength is low or in physiological settings. So, the current data support the idea that hydrophobic interactions are the most important, while also suggesting that electrostatics probably play a secondary or modulatory role instead of being completely absent.

On the other hand, changes in pH had a pronounced effect on the equilibrium of protein oligomerization, as shown in Figure (**5**). The effects of extreme pH conditions were particularly notable. At pH 10.0, the SEC chromatogram exhibited a peak eluting in the void volume (<10 mL), indicating partial aggregation of 3CLpro-WT. This behavior is consistent with previous studies reporting that aggregated proteins typically elute in the void volume of SEC columns, as their large size prevents entry into the resin pores [26]. Protein aggregation under extreme pH conditions is a well-documented phenomenon, arising from alterations

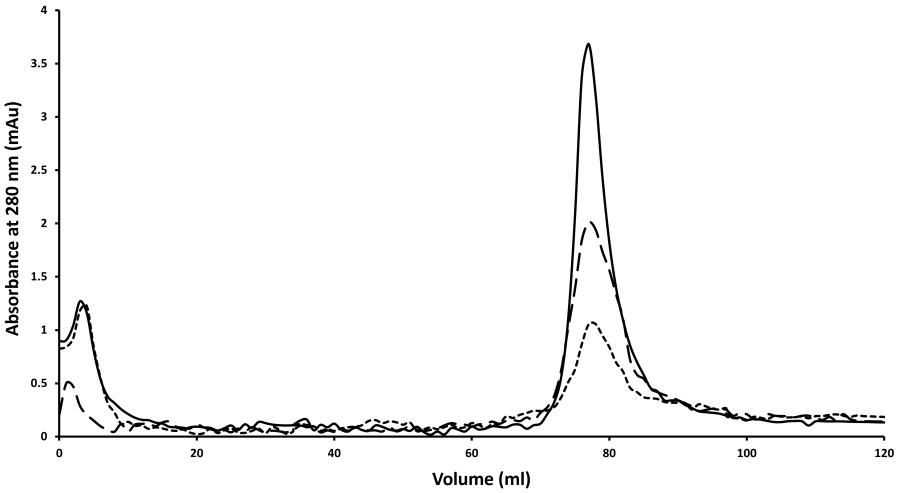

Figure 4. SEC chromatogram profile of 3CLpro-WT injected at a concentration of 2 mg/ml. The chromatogram depicts the elution of the protein in buffers with varying salt concentrations: 150 mM NaCl (dotted line), 300 mM NaCl (dashed line), and 500 mM NaCl (solid line). *(A higher resolution / colour version of this figure is available in the electronic copy of the article).*

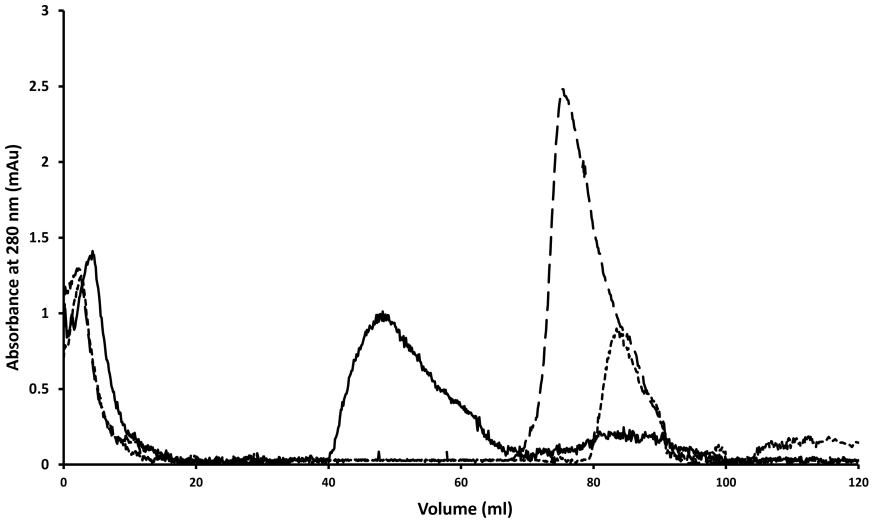

Figure 5. SEC chromatogram profile of 3CLpro-WT injected at a concentration of 2 mg/ml. The chromatogram displays the protein eluted with different pH buffers: pH 5.0 (dotted line), pH 8.0 (dashed line), and pH 10.0 (solid line). *(A higher resolution / colour version of this figure is available in the electronic copy of the article).*

in amino acid charge states that destabilize the native fold and promote non-specific hydrophobic interactions [27].

At pH 10.0, the elution profile also showed a distinct peak at approximately 50 mL, corresponding to an estimated molecular mass of ~150 kDa. This value is nearly fivefold higher than the theoretical monomeric mass of 3CLpro-WT (35 kDa). However, this could suggest the formation of a pentameric species; such a stable oligomeric state has not been reported for 3CLpro-WT. Therefore, it is more likely that this apparent pentameric species represents a transient and unstable oligomeric form that subsequently progresses toward aggregation, ultimately eluting in the void volume.

Collectively, these observations suggest that under alkaline conditions, 3CLpro-WT is unable to maintain its stable dimeric form, leading to structural destabilization, formation of higher-order oligomers, and eventual aggregation. A smaller peak was also observed at an elution volume of approximately 83 mL, corresponding to a molecular mass of ~40 kDa, which is close to the theoretical monomeric mass of 3CLpro-WT (35 kDa) [10]. This indicates that while the majority of the protein undergoes conformational changes and aggregation at pH 10.0, a minor fraction remains in the monomeric state. Taken together, these findings highlight that alkaline pH disrupts the dimeric interface of 3CLpro-WT, promoting transient monomer formation followed by higher-order oligomerization and aggregation. This confirms that 3CLpro-WT is structurally unstable upon dimer dissociation under alkaline conditions.

At a pH of 5.0, the elution profile demonstrated a notable shift towards a size approximating the monomeric form (about 38 kDa, elution volume of 85 mL). This evident change in elution time further substantiates that severe pH circumstances can destabilize the dimeric interface,

propelling the protein into a monomeric form. Significantly, in contrast to pH 10.0, the interruption of oligomerization at pH 5.0 did not lead to detectable aggregation, suggesting that the monomeric form of 3CLpro-WT is not intrinsically unstable at these conditions. The stability of the monomeric form at pH 5.0, even under severe pH conditions, contrasts with instances when monomeric forms are susceptible to rapid aggregation [3]. The persistent existence of the monomeric form of 3CLpro-WT at pH 5.0 reinforces the idea that the dimeric interface of this protein is considerably affected by ionic interactions between the two monomers. The divergent impacts of salt concentration and pH on the behavior of 3CLpro-WT in SEC profiles yield significant insights into the characteristics of its dimeric interface. The negligible effect of elevated salt concentrations (150–500 mM NaCl) on the elution profiles clearly corroborates the notion of the predominance of hydrophobic interactions in stabilizing the dimeric state. Hydrophobic interactions are often less affected by changes in ionic strength compared to electrostatic interactions [25, 28, 29]. The minimal impact of salt on dimerization indicates that hydrogen bonding, while possibly influential, has a comparatively insignificant role in preserving the overall stability of the dimeric structure [30].

In contrast, the notable impact of pH fluctuations on elution durations, especially at pH 5.0 and 10.0, suggests considerable structural alterations likely caused by protonation and deprotonation processes. The transition from a dimeric to a monomeric form under different pH circumstances validates the substantial role of ionic interactions at the dimeric interface. The aggregation noted at pH 10.0, along with the exclusive shift to a stable monomeric state at pH 5.0 without aggregation, potentially indicates a greater involvement of basic amino acids in the formation and stabilization of the dimeric interface, rather than acidic amino acids. At pH 10.0, which is considerably higher than the pKa values of most acidic residues (Asp ~3.65, Glu ~4.25) and approaching or exceeding the pKa of histidine (~6.0), yet remaining below that of lysine (~10.53) and arginine (~12.48), numerous basic residues would commence deprotonation. The reduction of positive charge may interfere with beneficial electrostatic interactions, resulting in protein destabilization and aggregation due to the exposure of hydrophobic regions [6, 12].

Conversely, at pH 5.0, acidic residues would primarily be protonated (neutral), whereas basic residues would generally stay protonated (positively charged). This modified charge distribution may result in electrostatic repulsion among monomers, leading to dissociation into stable, non-aggregating monomers. This thorough research, including the effects of pH and salt content, substantiates the claim that both hydrophobic and ionic interactions primarily facilitate the dimeric interface of 3CLpro-WT (Figure **6**). This study offers the first experimental validation of the critical contacts that facilitate dimerization, building on the precise residue profiles established by prior X-ray crystallography research [31]. This study unveils new opportunities for investigating alternate druggable locations within the interface, presenting interesting targets for rational drug design. Targeting hydrophobic, acidic, and basic residues for disruption could be an exceptionally effective method. The monomeric form of 3CLpro is known to lack catalytic activity. This study did not explicitly evaluate the catalytic activity of the isolated monomeric fraction; however, it is plausible to deduce, based on previous findings, that these monomers are enzymatically inactive [32].

3.3. Oligomeric state of 3CLpro WT: Effect of Concentration

The results of the SEC analysis also examined the impact of protein concentration on the oligomeric states of 3CLpro-WT. 3CLpro-WT demonstrated a distinct, albeit modest, peak that corresponded to the dimeric form at a protein concentration of 0.2 mg/ml, as illustrated in Figure (**7**). This discovery is in stark contrast to a previous investigation of SARS 3CLpro, which indicated that the compound existed exclusively in monomeric form at the same concentration [33]. Nevertheless, a separate investigation of SARS 3CLpro revealed a significant dimeric peak that corresponded with the present chromatogram. This indicates that the behavior of proteins at specific concentrations can be influenced by environmental factors [34]. The principal peak consistently

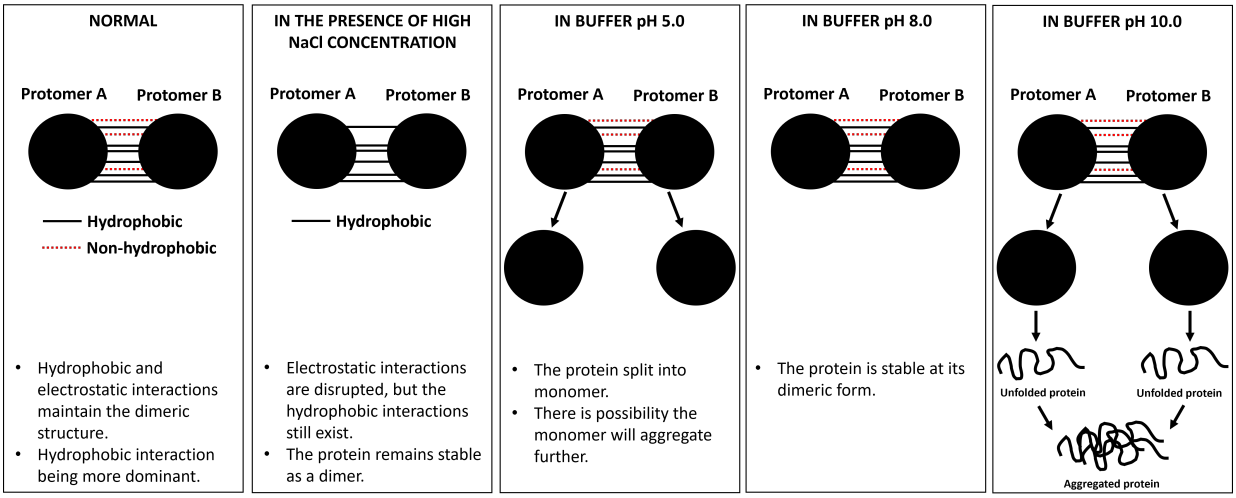

Figure 6. Hypothetical mechanism depicting the influence of salt and pH on the dimerization of 3CLpro-WT. *(A higher resolution / colour version of this figure is available in the electronic copy of the article).*

corresponded to the dimeric size of the protein (elution volume of 79 mL, with a size of 72 kDa), and the observed trend persisted at elevated concentrations of 2 mg/ml and 4 mg/ml. This consistency indicates that SARS-CoV-2 3CLpro has a higher propensity to form dimers and is not substantially influenced by its concentration, demonstrating Concentration-Independent Oligomerization (CIO). In biologically dimeric proteins, CIO is a common characteristic, indicating that they form stable dimers in their natural biological environment rather than solely under artificial *in vitro* conditions [14]. This behavior is in stark contrast to concentration-dependent oligomerization, in which molecular crowding is typically responsible for the formation of oligomeric structures [35]. The association of protein subunits into dimers is presumably driven by factors such as conformational changes or specific binding events in 3CLpro, regardless of their overall concentration [36-39]. This understanding has substantial implications for drug discovery, particularly in the context of the development of pharmaceuticals that disrupt dimerization. Strategies to prevent dimerization could target two stages, as a result of its biological dimeric nature: (1) early translation, which involves interfering with protein folding to prevent proper dimerization, and (2) post-translation, where medications target the properly folded dimeric form of 3CLpro.

3.4. Production of 3CLpro-ZM

Although the aforementioned experiments effectively identified the types of interactions that are essential for maintaining the stability of the 3CLpro dimeric structure, it is still imperative to identify specific target sites for disrupting this dimeric form in order to conduct focused drug discovery research. The significance of identifying a single or a limited number of specific sites for intervention is underscored by the significant complexity that is introduced by targeting multiple disruption sites. The structural feature that has been identified in 3CLpro is the Alanine-Valine knot, which is situated at the dimeric interface. This knot is particularly intriguing. A unique "zipper" arrangement with an approximate distance of 4.1 between the amino acids is formed by the hydrophobic interactions between Ala7 and Val125 of one monomer and Val125 and Ala7 of the opposing monomer within this knot. It is important to note that hydrophobic zippers are extensively documented in the literature, typically involving residues such as Leucine or Valine. However, the presence of an Alanine-Valine zipper is less frequently emphasized [14, 15]. Nevertheless, it is well-established that aliphatic hydrophobic residues, such as Alanine and Valine, are essential for protein dimerization [15]. Due to this, the Val/Ala zipper in 3CLpro probably plays a substantial role in its dimerization, rendering it a prospective target for impeding 3CLpro dimerization.

To experimentally investigate the functional role of this Ala7-Val125 zipper in the dimerization process and to determine if disrupting this knot could dissociate the homodimeric structure into monomers, a zipper mutant protein (3CLpro-ZM) was constructed. In this mutant, Alanine7 and Valine125 were simultaneously replaced by Glycine. This A7G/V125G mutation was hypothesized to substantially reduce the stability of the dimer interface, not only by removing the specific Ala-Val knot interactions but also by potentially introducing increased flexibility or unfavorable interactions at the interface due to Glycine's unique properties. Glycine, which contains a small H atom of the side chain, should exhibit greater conformational freedom compared to alanine or valine, which can destabilize helical structures or hydrophobic packing if introduced into specific structural contexts. The primary structure of this mutant protein is schematically shown in Figure (**8**), with the location of zipper residues illustrated in Figure (**9**).

The recombinant 3CLpro-ZM, which was fused with a 6xHis-tag at its C-terminal, was effectively expressed in a soluble form under the *E. coli* BL21(DE3) host cell. This was demonstrated by the presence of a distinct thick band in the supernatant following cell lysis (Figure **10**). Nevertheless, the mutant's overall protein level following expression was significantly lower than that of the wild-type enzyme, which indicated that the mutations may be destabilizing the protein and resulting in a more rapid

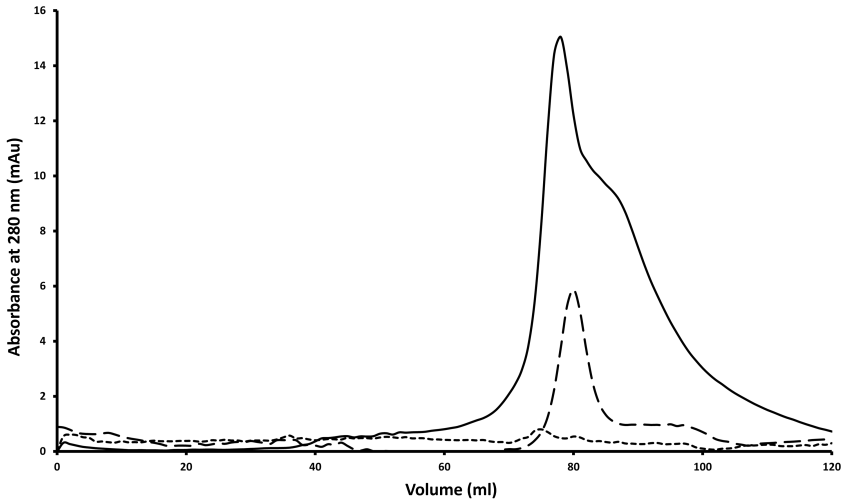

Figure 7. SEC chromatogram profiles of 3CLpro-WT injected at different concentrations: 0.2 mg/ml (dotted line), 2 mg/ml (dashed line), and 4 mg/ml (solid line). *(A higher resolution / colour version of this figure is available in the electronic copy of the article).*

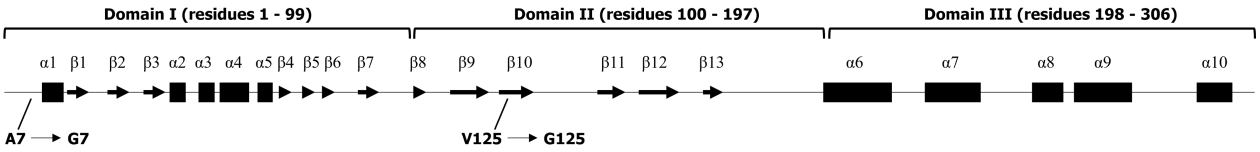

Figure 8. Schematic representation of the primary structure of 3CLpro-ZM. The α-helices and β-strands are represented by black boxes and arrows, respectively. This secondary structure is arranged based on the tertiary model of SARS-CoV-2 3CLpro (PDB ID: 6M03). The location of the mutated residues is also shown. *(A higher resolution / colour version of this figure is available in the electronic copy of the article).*

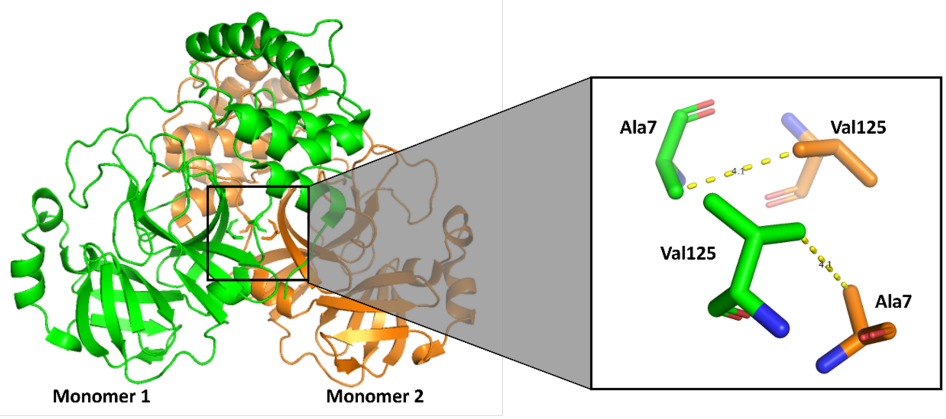

Figure 9. Three-dimensional structure of 3CLpro. The amino acid residues that make hydrophobic interactions at the dimer interface are indicated by stick models. *(A higher resolution / colour version of this figure is available in the electronic copy of the article).*

degradation. This observation is consistent with other investigations that have reported reduced expression levels and instability of mutant proteins [40]. It is also important to note that the apparent molecular mass of the zipper mutant (3CLpro-ZM) was significantly lower than the cumulative size anticipated for the MBP–3CLpro fusion construct. This observation suggests that the zipper mutant maintained autocatalytic activity that was adequate to facilitate the cleavage of the MBP tag and linker sequence during expression. Consequently, the 3CLpro-ZM protein that was the subject of subsequent experiments also exhibited a free N-terminus and a minimal C-terminal His tag.

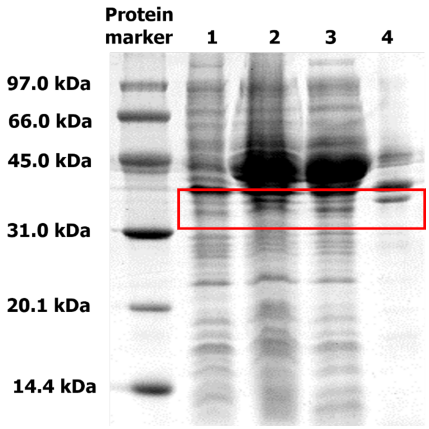

Figure 10. Expression check of 3CLpro-ZM visualized under 15% SDS-PAGE. Lane 1: Before IPTG induction; Lane 2: After IPTG induction; Lane 3: Soluble fraction obtained after the sonication; Lane 4: Insoluble fraction obtained after the sonication. The red box highlights the location of the recombinant proteins. *(A higher resolution / colour version of this figure is available in the electronic copy of the article).*

Further, the recombinant zipper mutant protein was effectively purified by a single-step Ni2+-NTA affinity chromatography, following a purification strategy that was substantially similar to that of 3CLpro-WT. A single band, which corresponds to its theoretical size of 35 kDa, was observed on a 15% SDS-PAGE gel, as illustrated in Figure **11**. No notable contaminant bands were observed. It is important to note that the purified 3CLpro-ZM's apparent size was consistent with the molar mass of SARS-CoV-2 3CLpro, which was determined from its amino acid sequence.

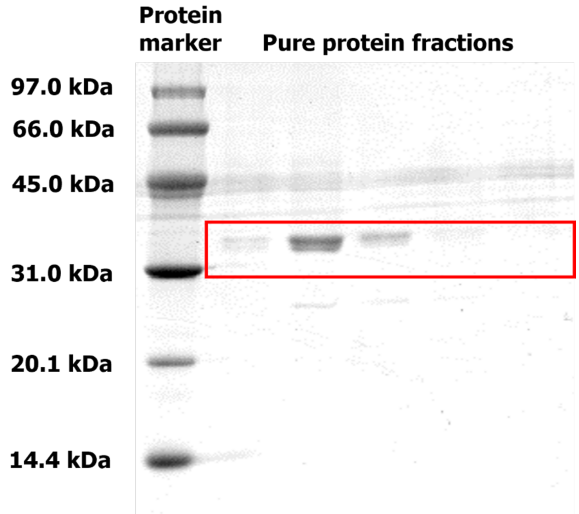

Figure 11. Purification checks of 3CLpro-ZM visualized under 15% SDS-PAGE after Ni^{2+}-NTA chromatography. *(A higher resolution / colour version of this figure is available in the electronic copy of the article).*

3.5. Far-UV Circular Dichroism (CD) Spectroscopy

The secondary structures and folding properties of the recombinant 3CLpro-ZM protein were evaluated using far-UV CD spectroscopy. The 3CLpro-ZM spectrum still exhibited characteristic minima at approximately 222 nm and a shoulder around 208 nm, despite the fact that its depth was shallower than that of the wild-type (Figure **12**). These characteristics suggest an α-helical content, which is estimated to contain approximately 49% α-helix, 14% β-sheet, and other structures, based on Yang's method [22, 23]. The shallower depth of the spectrum indicates that the mutation induced subtle yet significant conformational changes, despite the fact that the protein adopted a folded conformation. The mutated zip knot's critical role in the preservation of the overall protein architecture is likely the cause of these changes, which is consistent with the disruption of the pleated sheet structure. This result is particularly compelling, as the introduction of mutations in only two residues (A7G/V125G) had such a profound structural effect, indicating that the overall structure of this protein is heavily reliant on the integrity of the Val/Ala helix.

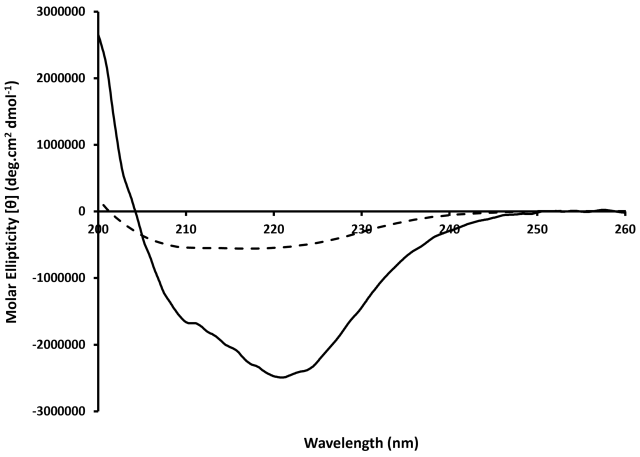

Figure 12. Far-UV CD spectra comparison between 3CLpro-WT (solid line) and 3CLpro-ZM (dashed line) was conducted at room temperature. *(A higher resolution / colour version of this figure is available in the electronic copy of the article).*

3.6. Enzymatic activity and Oligomeric State of 3CLpro-ZM

Consequently, the catalytic activity of 3CLpro-ZM was assessed to investigate enzymatic function. Protease activity was evaluated by utilizing a pNA substrate, specifically the 6-mer peptide TSAVLQ-pNA, which is cleaved by 3CLpro at the designated site (Gln-pNA) to liberate free pNA, resulting in an increase in absorbance at 405 nm [41]. The results demonstrated a substantial reduction in the enzymatic activity of 3CLpro-ZM in comparison to 3CLpro-WT (Table **2**). The wild-type enzyme exhibited a significantly higher specific activity than 3CLpro-ZM, which was determined to be 8.244 x 10-4 U/mg. In the same vein, the results of the esterase activity assessment using N-CBZ-Gly-pNP indicated that the catalytic activities of the two enzymes were highly comparable. 3CLpro-ZM exhibited a specific activity of 7.801 x 10-6 U/mg, which was significantly lower than the wild-type's 4.692 x 10-5 U/mg. The cleavage of both substrates was confirmed by the yellow color observed in the presence of the protein, which led to the production of free chromogenic pNA and pNP moieties [18].

Table 2. Specific activity comparison between 3CLpro-WT and 3CLpro-ZM.

Substrate	Specific activity of 3CLpro-WT (U/mg)	Specific activity of 3CLpro-ZM (U/mg)
TSALVQ-pNA	1.955×10^{-3}	8.244×10^{-4}
N-carbobenzoxyglycine p-nitrophenyl ester	4.692×10^{-5}	7.801×10^{-6}

3.7. Oligomeric State of 3CLpro-ZM

Furthermore, the oligomeric state of 3CLpro-ZM was analyzed by Size-Exclusion Chromatography (SEC) in the same manner as the wild-type protein, as shown in Figure **13**. At a protein concentration of 4 mg/mL, 3CLpro-ZM eluted at approximately 78 mL, which is comparable to the elution volume of 3CLpro-WT, indicating that both proteins predominantly exist in a dimeric form under these conditions. However, when the protein concentration was reduced to 2 mg/mL, the elution volume of 3CLpro-ZM shifted to approximately 83 mL, corresponding to an apparent molecular mass of ~40 kDa, which is close to the theoretical monomeric mass of 3CLpro (~35 kDa) (Figure **13**). This behavior contrasts with that of 3CLpro-WT, which remains predominantly dimeric across the tested concentration range.

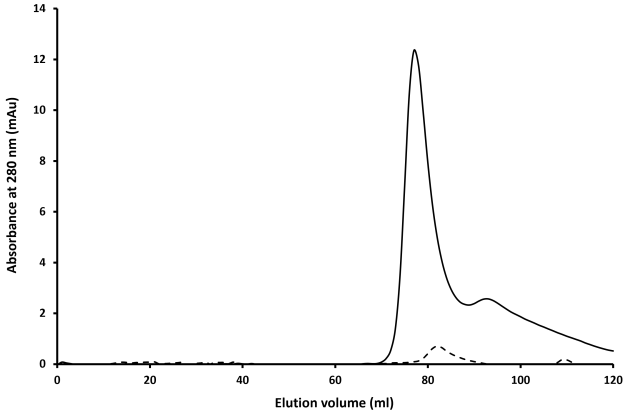

Figure 13. SEC chromatogram profiles of 3CLpro-ZM injected at different concentrations: 2 mg/ml (dashed line) and 4 mg/ml (solid line). *(A higher resolution / colour version of this figure is available in the electronic copy of the article).*

This concentration-dependent dissociation hypothetically suggests that disruption of the Ala7–Val125 zipper motif weakens the hydrophobic packing and inter-monomer contacts that stabilize the dimeric interface. At higher protein concentrations, mass action likely compensates for the reduced interfacial affinity, allowing transient dimer formation. In contrast, at lower concentrations, the weakened interface is insufficient to sustain stable dimerization, resulting in dissociation into monomers. These findings

indicate that the zipper motif plays a critical role in conferring concentration-independent dimer stability to 3CLpro, and its disruption shifts the equilibrium toward monomeric species under dilute conditions.

The reduction in catalytic activity of 3CLpro-ZM is likely explained by the observed shift in the monomer–dimer equilibrium, which is likely a key factor in conjunction with the enzymatic activity data. The A7G/V125G mutation disrupts the correct conformational state, particularly the formation of a stable dimer, which has been demonstrated to be essential for full protease activity, despite the fact that it does not completely abolish the overall folded structure of the protein [12]. The precise alignment of residues necessary to form a competent substrate-binding cleavage is likely impaired by destabilization of the dimeric interface, which substantially reduces enzymatic efficiency despite the preservation of a largely folded monomeric structure.

Notably, the dimeric structure of 3CLpro was previously reported to be crucial for the establishment of a precise substrate-binding cleavage between the two monomers [42]. The catalytic inactivity of monomeric 3CLpro has been consistently demonstrated, with the protein's functional state being the homodimer [32, 10]. Consequently, the A7G/V125G substitution appears to be a critical factor in the reduction of enzyme activity by disrupting the dimeric interface, despite the fact that it is not located at the catalytic site. This perturbation has the potential to impact the virus's pathogenicity and replication potency by reducing the protease's capacity to process viral polyproteins.

The Alanine-Valine knot, which is a critical structural determinant of 3CLpro, is present at the dimer interface. This knot is formed when the A7 and V125 of one monomer interact with the V125 and A7 of the other to form a zipper. Although the precise mechanism by which the A7G and V125G substitutions reduce 3CLpro-ZM enzyme activity is complex, it is strongly recommended that the mutation of these zipper amino acids impedes stable dimer formation and may impart local rigidity changes or alter hydrophobic packing at the interface. The smallest amino acid, glycine, incorporates substantial flexibility into protein structures. However, this flexibility can be destabilizing if it disrupts critical packing interactions or alters the conformational landscape necessary for stable dimerization. The substitution of larger, hydrophobic residues such as Alanine and Valine with Glycine would eliminate critical hydrophobic contacts and potentially introduce backbone flexibility that is incompatible with the precise geometry necessary for stable dimerization. It is crucial to emphasize that the Wild-type and mutant enzymes were both equipped with 6xHis tags at their C-terminus, which have been previously shown not disrupt the enzyme's dimeric structure or influence its activity [43, 41].

This investigation has revealed a highly promising approach to antiviral drug discovery: the inhibition of these specific residues. The Val/Ala knot's critical function in maintaining the overall protein architecture is emphasized by the significant conformational changes that are induced by the observed disruption of the interaction between these residues, which particularly affect the pleated sheet structure. This structural perturbation, in turn, considerably impedes the protein's capacity to dimerize effectively, thereby rendering it catalytically inactive. This mutation is spatially separated from the enzyme's direct catalytic site; however, it presents a viable and potentially highly effective approach to drug development when therapeutic efforts are directed toward the knot region. This allosteric approach has the potential to obstruct the virus's replicative capabilities, providing a novel and potent method to combat its proliferation and surmount the challenges associated with active-site inhibitors, such as drug resistance. It is important to acknowledge that the interface mutagenesis of 3CLpro, as reported in previous studies, has primarily focused on residues that are directly involved in hydrogen bonding, electrostatic interactions, or substrate-induced dimerization, particularly those that are proximate to the catalytic pocket. These investigations did not investigate whether minimal hydrophobic motifs constituted of small aliphatic residues could serve as critical structural anchors for dimer stability, despite the fact that they demonstrated that disruption of dimerization compromises enzymatic activity. The present findings contribute to this body of work by illustrating that the Ala7/Val125 zipper is crucial for the preservation of the enzyme's catalytic competence and conformational integrity, despite its spatial separation from the catalytic dyad. This underscores an allosteric vulnerability that was previously overlooked in the 3CLpro dimer interface. The mechanistic insights obtained in this investigation offer a clear framework for the rational development of antiviral agents targeting SARS-CoV-2 3CLpro from a translational perspective. In particular, the structure-guided design of small molecules or peptides that selectively disrupt this interface is made possible by the identification of the Ala7–Val125 zipper as a critical determinant of dimer stability. In this manner, these dimerization inhibitors could allosterically inactivate 3CLpro without directly engaging the catalytic site, thereby complementing the current active-site inhibitors. This approach has the potential to offer broad-spectrum antiviral activity against current and emerging SARS-CoV-2 variants and reduce the likelihood of resistance development, as the dimer interface is highly conserved across coronaviruses.

CONCLUSION

This study demonstrates that SARS-CoV-2 3CLpro predominantly exists as a stable homodimer in solution, with dimer stability largely maintained by hydrophobic interactions and modulated by pH-sensitive ionic contributions. Disruption of the Ala7–Val125 zipper through A7G/V125G mutation reduced protein stability, altered secondary structure, and significantly decreased protease and esterase activities, despite the mutant remaining folded. These findings indicate that the Ala7–Val125 interface is functionally important for maintaining the catalytically active dimeric state of 3CLpro. While no inhibitor studies were performed, the results support the dimer interface as a structurally relevant element that may be explored in future structure-guided antiviral design. In addition, unlike earlier interface mutagenesis studies that emphasized charged or substrate-binding residues, this work identifies a minimal alanine–valine hydrophobic zipper as a critical determinant of 3CLpro dimer stability and enzymatic function, revealing

a viable allosteric target for antiviral intervention. Nevertheless, despite providing important mechanistic insights into the role of the Ala7–Val125 zipper in 3CLpro dimer stability and activity, this study has several limitations. First, the assessment of 3CLpro oligomerization primarily relied on size-exclusion chromatography, which provides indirect estimates of molecular states and may not fully resolve transient or heterogeneous assemblies; complementary techniques such as analytical ultracentrifugation and native mass spectrometry would enable more definitive quantification of monomer–dimer equilibria. Second, only a single double mutant (A7G/V125G) was examined, limiting broader conclusions regarding the contributions of surrounding residues at the dimer interface. Third, although enzymatic assays demonstrated functional impairment, no direct inhibitor-binding studies or cellular validation were performed, leaving the physiological relevance and druggability of the Ala7–Val125 interface to be addressed in future work. Nevertheless, this study provides a solid foundation for subsequent future investigations, and the integration of structural, biophysical, and cell-based approaches will be essential to fully evaluate the therapeutic potential of targeting this allosteric interface.

AUTHORS' CONTRIBUTIONS

The authors confirm their contribution to the paper as follows: Study conception, design, supervision and final review of manuscript: C.B., V.K.; Data collection, preparation of first and final draft of the manuscript: R.R.; Data analysis and interpretation: C.B., R.R.; Data curation and funding acquisition: C.B., V.K. All authors reviewed the results and approved the final version of the manuscript.

LIST OF ABBREVIATIONS

3CLpro	=	3-Chymotrypsin-like Protease of SARS-CoV-2
3CLpro-WT	=	Wild-type SARS-CoV-2 3-chymotrypsin-like Protease
3CLpro-ZM	=	Zipper Mutant of SARS-CoV-2 3-chymotrypsin-like Protease (A7G/V125G)
SARS-CoV-2	=	Severe Acute Respiratory Syndrome Coronavirus 2
COVID-19	=	Coronavirus Disease 2019
SEC	=	Size-exclusion Chromatography
SDS-PAGE	=	Sodium Dodecyl Sulfate–polyacrylamide Gel Electrophoresis
CD	=	Circular Dichroism
Ni^{2+}-NTA	=	Nickel–nitrilotriacetic Acid Affinity Chromatography
Mpro	=	Main Protease of SARS-CoV-2
FPLC	=	Fast Protein Liquid Chromatography
OD600	=	Optical Density at 600 nm
MBP	=	Maltose-binding Protein
His-tag	=	Hexahistidine Affinity Tag
pNA	=	*p*-Nitroanilide
pNP	=	*p*-Nitrophenol
PDB	=	Protein Data Bank

ETHICS APPROVAL AND CONSENT TO PARTICIPATE

Not applicable.

HUMAN AND ANIMAL RIGHTS

Not Applicable.

CONSENT FOR PUBLICATION

Not applicable.

AVAILABILITY OF DATA AND MATERIAL

All data generated or analyzed during this study are included in this published article.

FUNDING

This work was financially supported by by UMS Great Grant (GUG0532-2/2022) and SDK0208-2020 from Universiti Malaysia Sabah.

CONFLICT OF INTEREST

The authors declare no conflict of interest, financial or otherwise.

ACKNOWLEDGEMENTS

The authors would like to acknowledge Dr. Andrey Kovalevsky (Oak Ridge National Laboratory, USA) for providing the recombinant plasmids of 3CLpro-CoV-2. This study is financially supported by Universiti Malaysia Sabah under GUG0532-2/2020 and SDK0208/2020.

AI DISCLOSURE STATEMENT

During the preparation of this manuscript, the authors used ChatGPT for language editing and grammar improvement. All AI-assisted content was carefully reviewed, verified, and revised by the authors to ensure accuracy, originality, and clarity. The authors take full responsibility for the integrity and final content of the published article.

REFERENCES

[1] Razali, R.; Asis, H.; Budiman, C. Structure-function characteristics of SARS-CoV-2 proteases and their potential inhibitors from microbial sources. *Microorganisms,* **2021**, *9*(12), 2481. http://dx.doi.org/10.3390/microorganisms9122481 PMID: 34946083

[2] Wu, F.; Zhao, S.; Yu, B.; Chen, Y.M.; Wang, W.; Song, Z.G.; Hu, Y.; Tao, Z.W.; Tian, J.H.; Pei, Y.Y.; Yuan, M.L.; Zhang, Y.L.; Dai, F.H.; Liu, Y.; Wang, Q.M.; Zheng, J.J.; Xu, L.; Holmes, E.C.; Zhang, Y.Z. A new coronavirus associated with human respiratory disease in china. *Nature,* **2020**, *579*(7798), 265-269. http://dx.doi.org/10.1038/s41586-020-2008-3 PMID: 32015508

[3] Khan, Z.; Karataş, Y.; Rahman, H. Anti COVID-19 drugs: Need for more clinical evidence and global action. *Adv. Ther.,* **2020**, *37*(6), 2575-2579.

http://dx.doi.org/10.1007/s12325-020-01351-9 PMID: 32350686

[4] Torner, N. The end of COVID-19 public health emergency of international concern (PHEIC): And now what? *Vacunas,* **2023**, *24*(3), 164-165. http://dx.doi.org/10.1016/j.vacun.2023.05.002 PMID: 37362832

[5] Owen, D.R.; Allerton, C.M.N.; Anderson, A.S.; Aschenbrenner, L.; Avery, M.; Berritt, S.; Boras, B.; Cardin, R.D.; Carlo, A.; Coffman, K.J.; Dantonio, A.; Di, L.; Eng, H.; Ferre, R.; Gajiwala, K.S.; Gibson, S.A.; Greasley, S.E.; Hurst, B.L.; Kadar, E.P.; Kalgutkar, A.S.; Lee, J.C.; Lee, J.; Liu, W.; Mason, S.W.; Noell, S.; Novak, J.J.; Obach, R.S.; Ogilvie, K.; Patel, N.C.; Pettersson, M.; Rai, D.K.; Reese, M.R.; Sammons, M.F.; Sathish, J.G.; Singh, R.S.P.; Steppan, C.M.; Stewart, A.E.; Tuttle, J.B.; Updyke, L.; Verhoest, P.R.; Wei, L.; Yang, Q.; Zhu, Y. An oral SARS-CoV-2 M^{pro} inhibitor clinical candidate for the treatment of COVID-19. *Science,* **2021**, *374*(6575), 1586-1593. http://dx.doi.org/10.1126/science.abl4784 PMID: 34726479

[6] Jin, Z.; Du, X.; Xu, Y.; Deng, Y.; Liu, M.; Zhao, Y.; Zhang, B.; Li, X.; Zhang, L.; Peng, C.; Duan, Y.; Yu, J.; Wang, L.; Yang, K.; Liu, F.; Jiang, R.; Yang, X.; You, T.; Liu, X.; Yang, X.; Bai, F.; Liu, H.; Liu, X.; Guddat, L.W.; Xu, W.; Xiao, G.; Qin, C.; Shi, Z.; Jiang, H.; Rao, Z.; Yang, H. Structure of M^{pro} from SARS-CoV-2 and discovery of its inhibitors. *Nature,* **2020**, *582*(7811), 289-293. http://dx.doi.org/10.1038/s41586-020-2223-y PMID: 32272481

[7] Pillaiyar, T.; Manickam, M.; Namasivayam, V.; Hayashi, Y.; Jung, S.H. An overview of severe acute respiratory syndrome–coronavirus (SARS-COV) 3CL protease inhibitors: Peptidomimetics and small molecule chemotherapy. *J. Med. Chem.,* **2016**, *59*(14), 6595-6628. http://dx.doi.org/10.1021/acs.jmedchem.5b01461 PMID: 26878082

[8] Morse, J.S.; Lalonde, T.; Xu, S.; Liu, W.R. Learning from the past: Possible urgent prevention and treatment options for severe acute respiratory infections caused by 2019-nCoV. *ChemBioChem,* **2020**, *21*(5), 730-738. http://dx.doi.org/10.1002/cbic.202000047 PMID: 32022370

[9] Zhang, D.; Chen, J.; Deng, L.; Mao, Q.; Zheng, J.; Wu, J.; Zeng, C.; Li, Y. Evolutionary selection associated with the multi-function of overlapping genes in the hepatitis B virus. *Infect. Genet. Evol.,* **2010**, *10*(1), 84-88. http://dx.doi.org/10.1016/j.meegid.2009.10.006 PMID: 19879378

[10] Goyal, B.; Goyal, D. Targeting the dimerization of the main protease of coronaviruses: A potential Broad-Spectrum therapeutic strategy. *ACS Comb Sci.,* **2020**, *22*(6), 297-305. http://dx.doi.org/10.1021/acscombsci.0c00058 PMID: 32402186

[11] Zhang, L.; Lin, D.; Sun, X.; Curth, U.; Drosten, C.; Sauerhering, L.; Becker, S.; Rox, K.; Hilgenfeld, R. Crystal structure of SARS-CoV-2 main protease provides a basis for design of improved α-ketoamide inhibitors. *Science,* **2020**, *368*(6489), 409-412. http://dx.doi.org/10.1126/science.abb3405 PMID: 32198291

[12] Chen, S.; Zhang, J.; Hu, T.; Chen, K.; Jiang, H.; Shen, X. Residues on the dimer interface of SARS coronavirus 3C-like protease: Dimer stability characterization and enzyme catalytic activity analysis. *J. Biochem.,* **2007**, *143*(4), 525-536. http://dx.doi.org/10.1093/jb/mvm246 PMID: 18182387

[13] Cai, X.; Wang, D.; Zhang, R.; Chen, Y.; Chen, J. The transmembrane domains of GPCR dimers as targets for drug development. *Drug Discov. Today,* **2023**, *28*(1), 103419. http://dx.doi.org/10.1016/j.drudis.2022.103419 PMID: 36309194

[14] Budiman, C.; Tadokoro, T.; Angkawidjaja, C.; Koga, Y.; Kanaya, S. Role of polar and nonpolar residues at the active site for PPIase activity of FKBP22 from *Shewanella* sp. SIB1. *FEBS J.,* **2012**, *279*(6), 976-986. http://dx.doi.org/10.1111/j.1742-4658.2012.08483.x PMID: 22244380

[15] Moitra, J.; Szilák, L.; Krylov, D.; Vinson, C. Leucine is the most stabilizing aliphatic amino acid in the d position of a dimeric leucine zipper coiled coil. *Biochemistry,* **1997**, *36*(41), 12567-12573. http://dx.doi.org/10.1021/bi971424h PMID: 9376362

[16] Kneller, D.W.; Phillips, G.; O'Neill, H.M.; Jedrzejczak, R.; Stols, L.; Langan, P.; Joachimiak, A.; Coates, L.; Kovalevsky, A. Structural plasticity of SARS-CoV-2 3CL M^{pro} active site cavity revealed by room temperature X-ray crystallography. *Nat. Commun.,* **2020**, *11*(1), 3202. http://dx.doi.org/10.1038/s41467-020-16954-7 PMID: 32581217

[17] Froger, A.; Hall, J.E. Transformation of plasmid DNA into *E. coli* using the heat shock method. *J. Vis. Exp.,* **2007**, (6), 253. http://dx.doi.org/10.3791/253 PMID: 18997900

[18] Razali, R.; Subbiah, V.K.; Budiman, C. Technical data of heterologous expression and purification of SARS-CoV-2 proteases using *Escherichia coli* system. *Data,* **2021**, *6*(9), 99. http://dx.doi.org/10.3390/data6090099

[19] Razali, R.; Kumar, V.; Budiman, C. Structural insights into the enzymatic activity of cysteine protease bromelain of MD2 pineapple. *Pak J. Biol. Sci.,* **2020**, *23*(6), 829-838. http://dx.doi.org/10.3923/pjbs.2020.829.838

[20] Laemmli, U.K. Cleavage of structural proteins during the assembly of the head of bacteriophage T4. *Nature,* **1970**, *227*(5259), 680-685. http://dx.doi.org/10.1038/227680a0 PMID: 5432063

[21] Chen, S.; Chen, L.; Tan, J.; Chen, J.; Du, L.; Sun, T.; Shen, J.; Chen, K.; Jiang, H.; Shen, X. Severe acute respiratory syndrome coronavirus 3C-like proteinase N terminus is indispensable for proteolytic activity but not for enzyme dimerization. Biochemical and thermodynamic investigation in conjunction with molecular dynamics simulations. *J. Biol. Chem.,* **2005**, *280*(1), 164-173. http://dx.doi.org/10.1074/jbc.M408211200 PMID: 15507456

[22] Chen, Y.H.; Yang, J.T. A new approach to the calculation of secondary structures of globular proteins by optical rotatory dispersion and circular dichroism. *Biochem. Biophys. Res. Commun.,* **1971**, *44*(6), 1285-1291. http://dx.doi.org/10.1016/S0006-291X(71)80225-5 PMID: 5168596

[23] Sreerama, N.; Woody, R.W. Estimation of protein secondary structure from circular dichroism spectra: Comparison of contin, selcon, and CDSSTR methods with an expanded reference set. *Anal. Biochem.,* **2000**, *287*(2), 252-260. http://dx.doi.org/10.1006/abio.2000.4880 PMID: 11112271

[24] Cheng, S.C.; Chang, G.G.; Chou, C.Y. Mutation of Glu-166 blocks the substrate-induced dimerization of SARS coronavirus main protease. *Biophys. J.,* **2010**, *98*(7), 1327-1336. http://dx.doi.org/10.1016/j.bpj.2009.12.4272 PMID: 20371333

[25] Baldwin, R.L. Energetics of protein folding. *J. Mol. Biol.,* **2007**, *371*(2), 283-301. http://dx.doi.org/10.1016/j.jmb.2007.05.078 PMID: 17582437

[26] Schägger, H Techniques and basic operations in membrane protein purification. In: Membrane Protein Purification and Crystallization, 2nd; Hunte, C; Von Jagow, G; Schägger, H, Eds.; Academic Press: San Diego, **2003**; pp. 19-53. http://dx.doi.org/10.1016/B978-012361776-7/50003-6

[27] Li, R.; Wu, Z.; Wangb, Y.; Ding, L.; Wang, Y. Role of pH-induced structural change in protein aggregation in foam fractionation of bovine serum albumin. *Biotechnol. Rep.,* **2016**, *9*, 46-52. http://dx.doi.org/10.1016/j.btre.2016.01.002 PMID: 28352591

[28] Dill, K.A. Dominant forces in protein folding. *Biochemistry,* **1990**, *29*(31), 7133-7155. http://dx.doi.org/10.1021/bi00483a001 PMID: 2207096

[29] Makhatadze, G.I.; Privalov, P.L. Energetics of protein structure. *Adv. Protein Chem.,* **1995**, *47*, 307-425. http://dx.doi.org/10.1016/S0065-3233(08)60548-3 PMID: 8561051

[30] Nick Pace, C.; Scholtz, J.M.; Grimsley, G.R. Forces stabilizing proteins. *FEBS Lett.,* **2014**, *588*(14), 2177-2184. http://dx.doi.org/10.1016/j.febslet.2014.05.006 PMID: 24846139

[31] Ferreira, J.C.; Fadl, S.; Rabeh, W.M. Key dimer interface residues impact the catalytic activity of 3CLpro, the main protease of SARS-CoV-2. *J. Biol. Chem.,* **2022**, *298*(6), 102023. http://dx.doi.org/10.1016/j.jbc.2022.102023 PMID: 35568197

[32] Abian, O.; Ortega-Alarcon, D.; Jimenez-Alesanco, A.; Ceballos-Laita, L.; Vega, S.; Reyburn, H.T.; Rizzuti, B.; Velazquez-Campoy, A. Structural stability of SARS-CoV-2 3CLpro and identification of quercetin as an inhibitor by experimental screening. *Int. J. Biol. Macromol,* **2020**, *164*, 1693-1703. http://dx.doi.org/10.1016/j.ijbiomac.2020.07.235 PMID: 32745548

[33] Fan, K.; Wei, P.; Feng, Q.; Chen, S.; Huang, C.; Ma, L.; Lai, B.; Pei, J.; Liu, Y.; Chen, J.; Lai, L. Biosynthesis, purification, and substrate specificity of severe acute respiratory syndrome coronavirus 3C-like proteinase. *J. Biol. Chem.,* **2004**, *279*(3), 1637-1642.

http://dx.doi.org/10.1074/jbc.M310875200 PMID: 14561748

[34] Kuo, C.J.; Chi, Y.H.; Hsu, J.T.A.; Liang, P.H. Characterization of SARS main protease and inhibitor assay using a fluorogenic substrate. *Biochem. Biophys. Res. Commun.,* **2004**, *318*(4), 862-867.
http://dx.doi.org/10.1016/j.bbrc.2004.04.098 PMID: 15147951

[35] Kuznetsova, I.; Turoverov, K.; Uversky, V. What macromolecular crowding can do to a protein. *Int. J. Mol. Sci.,* **2014**, *15*(12), 23090-23140.
http://dx.doi.org/10.3390/ijms151223090 PMID: 25514413

[36] Lim, C.P.; Cao, X. Structure, function, and regulation of STAT proteins. *Mol. Biosyst.,* **2006**, *2*(11), 536-550.
http://dx.doi.org/10.1039/b606246f PMID: 17216035

[37] Lees, J.A.; Saito, M.; Vidal, M.; Valentine, M.; Look, T.; Harlow, E.; Dyson, N.; Helin, K. The retinoblastoma protein binds to a family of E2F transcription factors. *Mol. Cell. Biol.,* **1993**, *13*(12), 7813-7825.
http://dx.doi.org/10.1128/MCB.13.12.7813 PMID: 8246996

[38] Chen, D.; Pace, P.E.; Coombes, R.C.; Ali, S. Phosphorylation of human estrogen receptor α by protein kinase a regulates dimerization. *Mol. Cell. Biol.,* **1999**, *19*(2), 1002-1015.
http://dx.doi.org/10.1128/MCB.19.2.1002 PMID: 9891036

[39] Mohammadi, M.; Olsen, S.K.; Ibrahimi, O.A. Structural basis for fibroblast growth factor receptor activation. *Cytokine Growth Factor Rev.,* **2005**, *16*(2), 107-137.
http://dx.doi.org/10.1016/j.cytogfr.2005.01.008 PMID: 15863029

[40] Iketani, S.; Hong, S.J.; Sheng, J.; Bahari, F.; Culbertson, B.; Atanaki, F.F.; Aditham, A.K.; Kratz, A.F.; Luck, M.I.; Tian, R.; Goff, S.P.; Montazeri, H.; Sabo, Y.; Ho, D.D.; Chavez, A. Functional map of SARS-CoV-2 3CL protease reveals tolerant and immutable sites. *Cell. Host Microbe,* **2022**, *30*(10), 1354-1362.e6.
http://dx.doi.org/10.1016/j.chom.2022.08.003 PMID: 36029764

[41] Huang, C.; Wei, P.; Fan, K.; Liu, Y.; Lai, L. 3C-like proteinase from SARS coronavirus catalyzes substrate hydrolysis by a general base mechanism. *Biochemistry,* **2004**, *43*(15), 4568-4574.
http://dx.doi.org/10.1021/bi036022q PMID: 15078103

[42] Chuck, C.P.; Chong, L.T.; Chen, C.; Chow, H.F.; Wan, D.C.C.; Wong, K.B. Profiling of substrate specificity of SARS-CoV 3CL. *PLoS One,* **2010**, *5*(10), e13197.
http://dx.doi.org/10.1371/journal.pone.0013197 PMID: 20949131

[43] Chou, C.Y.; Chang, H.C.; Hsu, W.C.; Lin, T.Z.; Lin, C.H.; Chang, G.G. Quaternary structure of the severe acute respiratory syndrome (SARS) coronavirus main protease. *Biochemistry,* **2004**, *43*(47), 14958-14970.
http://dx.doi.org/10.1021/bi0490237 PMID: 15554703